RSC Advances

ROYAL SOCIETY OF CHEMISTRY

PAPER

View Article Online
View Journal | View Issue

Check for updates

Cite this: *RSC Adv.*, 2023, **13**, 5946

Highly water-stable, luminescent, and monodisperse polymer-coated $CsPbBr_3$ nanocrystals for imaging in living cells with better sensitivity†

Manav Raj Kar,[a] Shamit Kumar,[b] Tusar Kanta Acharya,[b] Chandan Goswami[b] and Saikat Bhaumik *[a]

Received 5th November 2022
Accepted 13th February 2023

DOI: 10.1039/d2ra07019g

rsc.li/rsc-advances

Recently, $CsPbX_3$ (X= Cl, Br, I) nanocrystals (NCs) have evolved as a potential contender for various optoelectronic applications due to some of their excellent photophysical properties. Their superior non-linear optical properties enable them to take part in bioimaging applications due to their longer penetration depth and less scattering effect in living cells. However, the poor stability of perovskite NCs in aqueous media still remains a great challenge for practical usage. Comparatively stable silica-coated NCs have a tendency to agglomerate among other NCs and transform into bigger particles. Such big particles clog the inside of narrow channels during the uptake and can't effectively reach the targeted cells. To tackle such issues, we introduce a fast and reproducible synthesis process of $CsPbBr_3$ NCs that are coated with different long-chained organic ligands/polymers and compared their photophysical properties. Among them, polyvinylpyrrolidone (PVP) encapsulated NCs are highly luminescent in the green spectral region and showed a maximum photoluminescence quantum yield (PLQY) of up to 84%. The incorporation of *n*-isopropyl acrylamide (NIPAM) along with PVP further improves the stability of the PVP-coated NCs against heat and moisture. These NCs exhibit higher water stability compared to silica-coated NCs and maintained their emission properties for about one week in DI water. The smaller particle size, uniform size distribution, higher structural stability, and better dispersivity of polymer-coated NCs in the aqueous media enable them to perform as fluorescent probes for live cell imaging in mammalian Chinese Hamster Ovary (CHO-K1) cells. There is no adverse affect in the cells' viability and morphology even after long incubation periods (~72 hours). The dosage of Pb-ions contained in the polymer-coated NCs is calculated as below 5 $\mu g\ mL^{-1}$, which is suitable for live cell imaging. This work provides insight for expanding the use of these NCs significantly into bioimaging applications with higher sensitivity.

1. Introduction

Semiconducting nanocrystals (NCs) have emerged as a new alternative for bioimaging and diagnostic applications due to their unique photophysical properties, such as high photoluminescence (PL) intensity, and superior stability, multiphoton absorption, and more resistance to photo-bleaching.[1–7] The NCs generally process higher surface-to-volume ratios allowing easy surface modifications in order to increase their reactivity, solubility, and biocompatibility.[8–10] The ligands bound to the NCs surface influence the physical and photophysical properties of the nanoparticles. Ligands usually passivate the NCs' surface and improve colloidal stability and emission intensity in different ranges of biological media.[11–13] NCs conjugated with specific ligands are tested for targeting particular cells with high selectivity. The usage of NCs as drug carriers is a potential strategy for improving drug-delivery system efficiency and lowering pharmacological side effects.[14–16] The NCs are of utmost importance for biomedical fields since many proteins and biomolecules exist in similar size ranges that are not accessible with large particles.[17–20] The smaller size of NCs also enables higher detection specificity, selectivity, and intracellular uptake capacity.

Recently, $CsPbX_3$ (X= Cl, Br, I) perovskite NCs have become a popular fluorescent material with great potential in various optoelectronic devices.[21–28] These perovskite NCs also possess some unique properties that prove to be fruitful in bioimaging

---

[a] *Department of Engineering and Materials Physics, Institute of Chemical Technology-IndianOil Odisha Campus, Mouza-Samantapuri, Bhubaneswar, 751013, Odisha, India. E-mail: s.bhaumik@iocb.ictmumbai.edu.in*

[b] *School of Biological Sciences, National Institute of Science Education and Research, Bhubaneswar, 752050, Odisha, India*

† Electronic supplementary information (ESI) available. See DOI: https://doi.org/10.1039/d2ra07019g

applications, such as (i) a simple colloidal and post-synthesis process with adaptable bioconjugation strategy; (ii) tunable bandgap with multi-colored optical imaging capability; (iii) narrow emission spectra with a full-width at half maximum (FWHM), which promote multiple resolutions of fluorescent probes simultaneously. The perovskite NCs demonstrates a great potentiality for multiphoton applications due to their high nonlinear optical cross-section.[29–31] The $CsPbX_3$ NCs are generally synthesized *via* the hot injection synthesis method which is complex and time-taking.[32,33] Ligand-assisted reprecipitation (LARP) is a more facile method for the synthesis of $CsPbX_3$ NCs at room temperature.[34,35] Long-chained organic ligands like oleic acid (OAc) and oleylamine (OAm) are commonly employed as primary surface capping agents for $CsPbX_3$ NCs.[36–38] These ligands are weakly bound to the NCs surface which increases the density of surface trap states and damages the crystal structure. Doping of metal ions and silica-coating around the perovskite NCs execute better stability with superior optical properties and are successfully implemented in bioimaging applications.[39–43] This synthesis method also facilitates the growth of nonluminous Cs_4PbBr_6 perovskite phases that overall reduces the NCs emission intensity.[42,44] However, their bigger particle size and tendency to agglomerate among other NCs,[45–47] cause adverse effects on cellular uptake in deep tissues due to the trapping in cellular channels.[48,49] Overall superior luminescent properties, smaller particle size, and excellent water stability are some essential features that a luminescent probe must possess for high and sensitive bioimaging applications.[50–52]

Encapsulation of perovskite NCs with different functionalized polymers is also an alternative method for the protection of the core perovskite materials from the external harsh environment.[53–55] Different bio-compatible polymer-coated perovskite NCs were often preferred to ensure low cytotoxicity, higher stability, and easy uptake in the cells.[56–59] Polyvinylpyrrolidone (PVP) polymer contains strongly hydrophilic pyrrolidone moiety and hydrophobic alkyl groups that prevent the aggregation of NCs due to their repulsive forces.[60,61] PVP forms an ultrathin shell around the NCs surface *via* adsorption which can easily detach under external stress. An additional suitable coating/binding is required around PVP-coated NCs that can maintain the particle size and improve crystal stability, which is of utmost importance for a practical bioimaging application. Recently, PVP polymers were used as a surfactant for stabilizing the $CsPbX_3$ NCs and also served as an interfacial layer for making them compatible with the coating of poly(-methyl methacrylate) [PMMA] and polystyrene (PS) polymers.[56,59] However, the sizes of these nanocomposites are very large (~μm range) due to the uncontrolled coating of polymers over the PVP layer, reducing the uptake efficiency in the cells. Poly[*n*-isopropyl acrylamide] (pNIPAM) is an extensively instigated thermosensitive biocompatible polymer with a lower critical solution temperature and has been widely utilized as a polymer hydrogel in the field of biomedical applications, such as cancer cell imaging, drug carriers, and biosensors.[62–64] However NIPAM monomers can also act as binding agents due to the presence of specific functional groups and hence result in passivation of NCs and thus improve stability.[65] The secondary amide of NIPAM makes them stronger H-bond acceptors compared to primary amide groups and the presence of the lipophilic isopropyl group is responsible for its high solubility in nonpolar solvents.[66]

Herein, we report the synthesis of $CsPbBr_3$ perovskite NCs *via* the LARP synthetic approach that was coated with different stable materials. We introduced biocompatible PVP polymer and functional NIPAM monomer as protective layers around the perovskite NCs and compared the photophysical properties with conventional $CsPbBr_3$ NCs. These NCs emit green emission spectra and reached a maximum PLQY of up to 84%. The conventional long-chained organic OAc-OAm capped $CsPbBr_3$ NCs degrade very fast in polar solvents. Comparatively stable silica-coated NCs agglomerate among themselves and become bigger particles with time which is not favorable for bioimaging applications. So, we introduce PVP-coated $CsPbBr_3$ NCs which in addition to NIPAM exhibited smaller particle sizes, were less prone to agglomeration effect, and had higher stability toward the water and heat, enabling them to use as a fluorescent probe for live cell imaging in mammalian Chinese Hamster Ovary (CHO-K1) cells. The effective coating of PVP polymer also reduces the toxicity of NCs towards cells, and no notable changes in cellular structure or cell organelles like lysosomes and mitochondria were noticed even after prolonged incubation periods (~72 hours).

2. Results and discussion

The $CsPbBr_3$ NCs were synthesized *via* the LARP synthetic method under normal atmospheric conditions.[67] The detailed synthesis process is discussed in the ESI† part. Here, The CPB-1 NCs were synthesized by injecting a mixed precursor of CsBr, $PbBr_2$, OAc, OAm, and dimethylformamide (DMF) in a toluene solvent under vigorous stirring conditions. For the synthesis of CPB-2 NCs, we introduced *n*-octylammonium bromide (OABr) powder in the precursor and followed the same synthesis method for the synthesis of CPB-1 NCs. CPB-3 and CPB-4 NCs were synthesized by injecting the same precursor for synthesis of CPB-2 NCs, while PVP polymer and PVP along with NIPAM were premixed in the toluene before injection of the respective precursors, respectively. Silica-coated $CsPbBr_3$ NCs were synthesized *via* a similar LARP method where (3-aminopropyl) triethoxysilane (APTMS) was chosen as a silica source.[42,68] A longer synthesis time for silica-coated NCs is required for the completion of the hydrolysis process of alkoxysilane groups present in APTMS to form silanol groups that cover the NCs surface.

The UV-vis absorption spectra of the NCs in the solution phase are shown in Fig. 1a. The absorption spectra reveal a band edge absorption peak at around 513 nm for all NCs denoting the presence of 3D $CsPbBr_3$ perovskite phases. In addition, a sharp absorption peak appears at 320 nm, which signifies the presence of 0D Cs_4PbBr_6 phases.[42,68] The absorption peak intensity of Cs_4PbBr_6 phases in CPB-1 NCs is significantly high as compared to other NCs. There are no observable shifts in absorption peaks noticed for the NCs. The PL emission

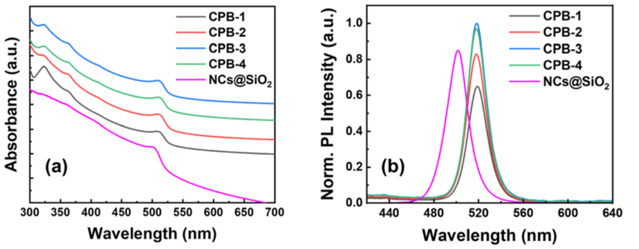

Fig. 1 Stacked (a) absorption and (b) PL spectra of CPB-1, CPB-2, CPB-3, CPB-4 NCs, and silica-coated $CsPbBr_3$ NCs, as represented in the legends.

spectra of the NCs are shown in Fig. 1b. The emission spectra of all NCs are observed at nearly the same position with a similar pattern. The emission peaks of all the NCs are obtained at around 519 nm with a FWHM of around 18 nm. The PLQY of CPB-1, CPB-2, CPB-3, and CPB-4 NCs were calculated as 55, 70, 84, and 82%, respectively. The PL intensity of CPB-1 NCs is low due to the presence of dynamic ligands that cannot passivate the NCs' surface effectively. It allows the formation of surface trap states that don't contribute to the radiative recombination.[69] The PL intensity of CPB-2 NCs increased as compared to CPB-1 NCs due to the formation of a very thin high bandgap 2D $(OA)_2PbBr_4$ shell layer around the NCs in presence of OABr precursor during synthesis that reduces the surface trap states and improves radiative recombination process.[67] Further incorporation of PVP and PVP-NIPAM mixture resulted in further enhancement in PL intensities of CPB-3 and CPB-4 NCs, which signifies the effective passivation of the NCs surface with the polymer coating.[69] The silica-coated $CsPbBr_3$ NCs reveals a band edge absorption peak at 500 nm and emission peak at 502 nm with a wider FWHM of 22 nm (see Fig. 1a and b). These NCs showed an emission PLQY of 72%. Strikingly, the PLQY values measured from different batches of polymer-coated NCs were closer to each other as compared to silica-coated $CsPbBr_3$ NCs, denoting a higher reproducibility of our synthesis process from batch to batch.

The X-ray diffraction (XRD) patterns of different perovskite NCs in the thin-film form are represented in Fig. 2. The XRD diffraction patterns for all the NCs thin-film reveal mixed perovskite phases of monoclinic $CsPbBr_3$ (PDF #00-18-0364) and rhombohedral Cs_4PbBr_6 (PDF #01-73-2478) crystal phases, which are matching quite well with the reference diffraction peaks.[42,70–72] The CPB-1 NC's diffraction pattern shows a higher contribution of Cs_4PbBr_6 phases as compared to $CsPbBr_3$ phases. CPB-1 NCs are encapsulated with OAc and OAm ligands which are dynamic in nature and do not bind tightly at NCs surface. The presence of excess OAm ligands in NCs solution facilitates the degradation of $CsPbBr_3$ NCs and transforms them into unwanted Cs_4PbBr_6 phases.[73] This overall reduces the perovskite NCs quality and emission properties. However, the contribution of Cs_4PbBr_6 phases decreases successively for CPB-2, CPB-3, and CPB-4 NCs, respectively. The introduction of OABr and polymer inhibits the degradation of perovskite NCs as they are forming protecting shells around NCs. The presence of $(OA)_2PbBr_4$ crystal phase is not detected in the XRD diffraction pattern due to a very thin shell layer formed around the NCs and their contribution is very less as compared to other crystal phases.

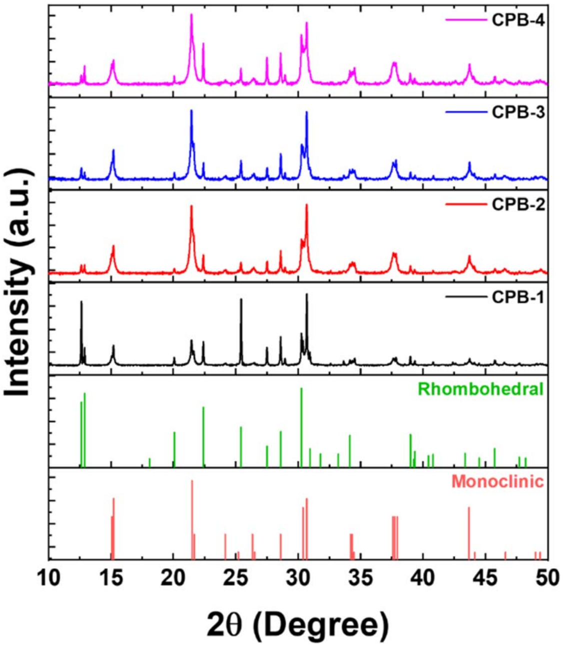

Fig. 2 Stacked XRD diffraction patterns of CPB-1, CPB-2, CPB-3, CPB-4 NCs in thin-film form. The bottom of the Figure represents the standard XRD diffraction patterns of monoclinic $CsPbBr_3$ and rhombohedral Cs_4PbBr_6 perovskite phases.

The shape and size of the NCs were investigated using transmission electron microscopy (TEM) imaging and corresponding images are shown in Fig. 3a–d. These images reveal that the NCs are cubic in shape and highly crystalline in nature. The maximum number of these NCs have edge size in the range of 12–20 nm and corresponding size distributions are shown in Fig. S1 (in ESI†). The CPB-1 and CPB-2 NCs showed a tendency for agglomeration among other NCs, resulting in non-uniform particle size distribution (see Fig. 3a and b). The presence of PVP and NIPAM at the surfaces of CPB-3 and CPB-4 NCs reduces the NCs agglomeration and exhibits monodisperse particle size distribution (see Fig. 3c–d). Among them, CPB-4 NCs demonstrate the best uniformity in NCs size distribution and are well dispersed to each other. This is beneficial for the strong confinement of charge carriers inside the NCs and enhances the NCs emission properties. The HRTEM image of CPB-4 NCs reveals a highly crystalline nature having an interplanar spacing of 0.42 nm (see Fig. S1a, in ESI†) that corresponds to (110) lattice plane for monoclinic $CsPbBr_3$ crystal structure.[74] We have also recorded the TEM image of conventional silica-coated $CsPbBr_3$ NCs as shown in Fig. 3e. The silica-coated $CsPbBr_3$ NCs are irregular in shape with particle size distribution in the range of 20–40 nm. The blurred surface around these perovskite NCs appeared from the adsorption of the compact silica shells. These NCs are prone to agglomerate among themselves and transform into big agglomerated structures. We further

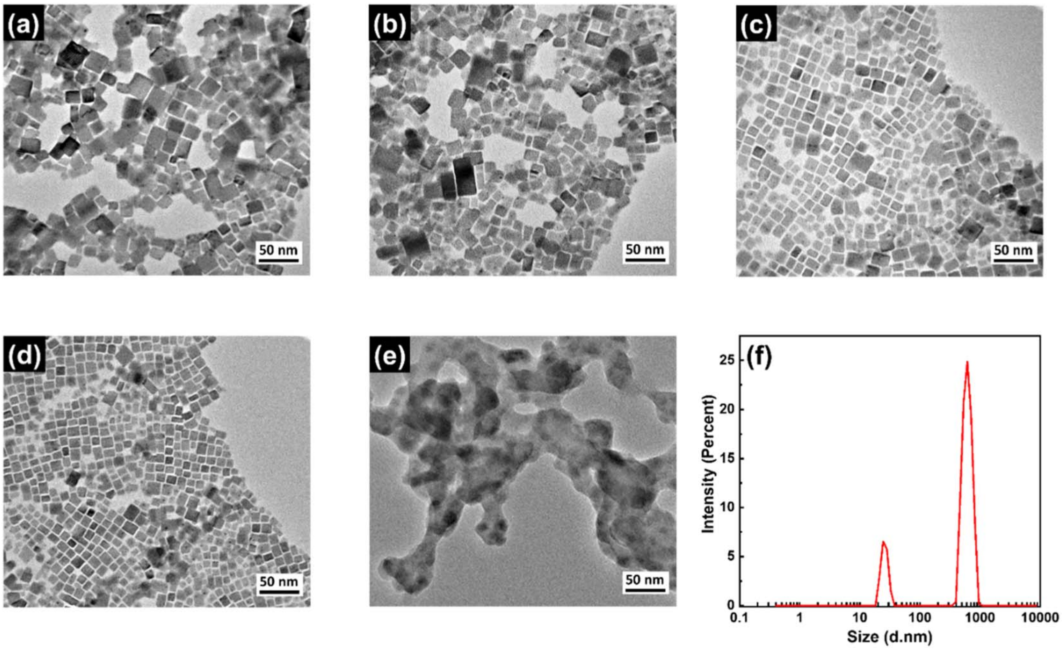

Fig. 3 TEM images of (a) CPB-1, (b) CPB-2, (c) CPB-3, (d) CPB-4 NCs, and (e) silica-coated $CsPbBr_3$ NCs. (f) DLS analysis of silica-coated $CsPbBr_3$ NCs.

confirmed the particle sizes of the silica-coated NCs by dynamic light scattering (DLS) measurements.[75] The DLS analysis of these NCs reveals the presence of clumped aggregation of NCs in a silica matrix as large as several hundred nm (see Fig. 3f). There are actually two size distributions of particles; one of lower intensity at 24.4 nm that appeared from the individual perovskite NCs. While intense peak at 615 nm indicates that the maximum particles aggregated to form larger particle sizes which is also confirmed from TEM imaging.

We have recorded the Fourier-transform infrared (FTIR) spectra of the NCs to identify the passivating agents around the NCs' surface. The corresponding FTIR spectra of all NCs are shown in Fig. 4a. The FTIR spectra of all NCs reveal strong absorption peaks at 1465, 3025, and 1740 cm^{-1} that originated from –COO–, –OH, and C=O functional groups due to the presence of the OAc capping ligand, and the additional peak at 1575 cm^{-1} appears from the N–H bending of the OAm capping ligand.[37,38] These results signify that the OAc and OAm ligands are present around all the NCs. However, CPB-3 and CPB-4 NCs exhibit some other absorption peaks along with the peaks of OAc and OAm capping ligands. The absorption peaks at 1290, 1440, and 1645 cm^{-1} represent the C–N stretching, C–H bending, and C=O stretching bonds of PVP polymer that are attached around the NCs surface.[59,68,76] CPB-4 NCs spectrum reveals furthermore peaks at 2890 and 3390 cm^{-1} that originated from C–H symmetric stretching and N–H stretching bonds, along with the peaks at 3208 cm^{-1} and 1580 cm^{-1} representing N–H stretching and N–H bending vibrations of NIPAM.[77,78] The absorption peak intensities at 1645 and 3390 cm^{-1} became intense with the introduction of NIPAM into the NCs (*i.e.*, CPB-4 NCs) as compared to the NCs without NIPAM (*i.e.*, CPB-3 NCs), revealing stronger C=O bonding interactions and N–H bending vibrations, respectively. Here, the C=O group of PVP interacts with N–H group of NIPAM *via* hydrogen bonding to form a compact layer of polymer shell. Similar observation was noticed for interaction of PVP with other species containing similar N–H groups.[79,80] The enhancement of absorption peaks at 1465 and 1575 cm^{-1} suggests that the polymer coating around the NCs improves the bonding of OAc and OAm ligands with the NCs surface.

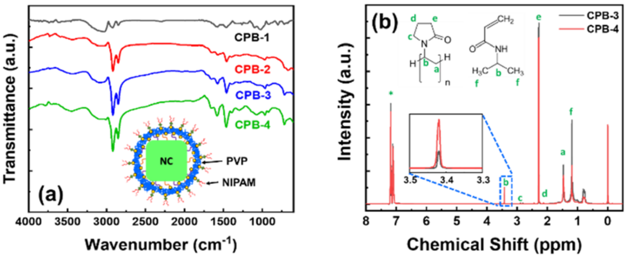

Fig. 4 (a) FTIR spectra of CPB-1, CPB-2, CPB-3, and CPB-4 NCs. Inset: schematic diagram of CPB-4 NCs that is coated with PVP and NIPAM. (b) NMR spectra of CPB-3 and CPB-4 NCs, as shown in legend (* indicates NMR peak of solvent). Inset: zoomed NMR spectra of the NCs.

We conducted nuclear magnetic resonance (NMR) spectroscopy of CPB-3 and CPB-4 NCs in deuterated-chloroform and the resultant 1-D ^1H NMR spectra are shown in Fig. 4b. This characterization technique is usually considered to understand the binding ability of a mixture of different ligands with the NCs. The NMR spectra for CPB-3 and CPB-4 NCs seem identical and no such detectable chemical shift is noticed. The chemical shifts less than 2.2 ppm are originated due to alkyl chains of the organic capping ligands and polymer.[37,38,81] The resonance signals for methylene (^{a}CH$_2$) and methine (^{b}CH) protons of PVP polymer are obtained at $\delta = 1.47$ and 3.41 ppm, respectively. Moreover, the resonance peaks obtain at $\delta = 2.2$ (^{e}CH$_2$) and 2.88 ppm (^{c}CH$_2$) indicate shifting of resonance peaks for –CH$_2$ groups attached to C=O group and adjoining –N atom, respectively. The downfield chemical shifts (~0.5 ppm) of CH$_2$ groups that bonded with N–C=O of acylamino groups in CPB-3 NCs as compared to pure PVP, can be attributed to the interactions between the N–C=O of acylamino and Cs$^+$-ions of the CsPbBr$_3$ perovskites that exposed to the NCs surface.[82] The resonance signals for $\delta = 3.41$ (^{b}CH) and 1.11 ppm (^{f}CH$_3$) are appeared from methine and methyl protons of NIPAM.[83,84] Moreover, the spectra of CPB-4 NCs shows reduction in resonant signal intensities at $\delta = 2.2$, 1.47, and 1.11 ppm, indicating increase in ligand binding and bonding interactions.[81] The increase in resonant signal at $\delta = 3.41$ ppm is appeared as a result of interaction between NIPAM with PVP.[83]

From the observations from FTIR and NMR spectra, it can be considered that the CsPbBr$_3$ NCs are capped with the functional groups of OAc and OAm ligands that are bonded with outermost Pb, Br-ions, respectively. The Cs-ions are interacted with C=O groups of PVP and the polymer chains form mesh-like coating that covers the entire NCs surface (see inset of Fig. 4a). The C=O groups of PVP are directed in both outward and inward directions of the mesh-like coating. The inner C=O groups of PVP chemically interacted with the outermost Cs-ions of the NCs, while the outer C=O groups attach with N–H groups of NIPAM *via* hydrogen bonding which evident from increase in signal intensity at 3.41 ppm (see inset of Fig. 4b). The compact PVP coating also prevents detachment of OAc and OAm ligands from NCs surface. Such chemical structure around the NCs significantly improves the stability.

Higher water stability of NCs is preliminarily required for practical bioimaging application in live cells. We studied the water stability of these NCs both in the solution phase and thin-film form. In the first case, we dispersed each NCs powder in separate vials containing DI water while maintaining the same concentration and then recorded the change in PL intensities with respect to time. The normalized PL intensities of the NCs over regular time intervals are shown in Fig. 5a and Fig. S2 (in ESI†). The photographic images of the NCs solutions dispersed in DI water with respect to time under a UV lamp are shown in Fig. 5c. The PL intensities of all the NCs decrease continuously over time because the water molecules accelerate the degradation process of the perovskite structures.[85,86] The CPB-1 NCs degraded very fast where 93% of PL intensity was quenched within 5 min. It reveals that the dynamic OAc and OAm ligands of CPB-1 NCs are not sufficient to protect the perovskite materials against water. The PL intensities of CPB-2 and CPB-3 NCs quenched 80% of their initial PL intensities after 45 and 60 min, respectively. However, the CPB-4 NCs retain almost 75% its initial PL intensity after 60 min and are luminescent under a UV lamp nearly 1 week. The water stability of these NCs (*i.e.*, CPB-2, CPB-3, CPB-4 NCs) significantly improves with addition of OABr and the polymers during the NCs synthesis, form protecting shells that resist the interaction of perovskite materials from water.[69]

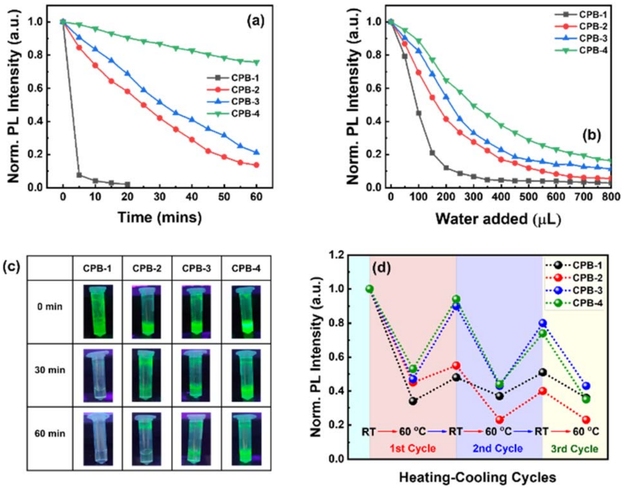

Fig. 5 The decay curves represent the decrease in PL intensities of CPB-1, CPB-2, CPB-3, and CPB-4 NCs after the addition of DI water as a function of (a) time and (b) amount of water added, as shown in legends. (c) Photographic images of the NCs solutions in water under a UV lamp that were captured at different time intervals. (d) Heating and cooling cycles of CPB-1, CPB-2, CPB-3, and CPB-4 NCs films, as shown in legend.

In another water stability test, we took 100 μL of each NCs solution (~10 mg mL^{-1}) in separate glass vials containing toluene followed by consecutive addition of 50 μL DI water in sequence followed by stirring and sonication. Then, we recorded the amount of DI water required to completely quench the emission intensity of each NCs solution. The corresponding change in normalized emission intensity of CPB-1, CPB-2, CPB-3, and CPB-4 NCs are shown in Fig. 5b and Fig. S3 (ESI†). Here also the CPB-1 NCs degraded at a much faster rate as compared to other NCs. The PL intensity of CPB-1 NCs was quenched by 55 and 90% of its initial PL intensity after the addition of 100 and 200 μL DI water, respectively. Similarly, the emission intensities of CPB-2, CPB-3, and CPB-4 NCs were decreased by 59, 46, and 36%, respectively after the addition of 200 μL DI water. In the second case, we tested the water stability of the NCs in thin-film form. In this regard, we drop-casted the NCs solutions on separate glass substrates and then immersed them in a glass beaker containing DI water. The PL spectra of the corresponding NCs films were recorded at regular time intervals. The photographic images of these NCs films in DI water under a UV lamp with time intervals of 60 min are shown in Fig. S4 (ESI†). As earlier, the CPB-1 NCs films quenched much faster than other films while CPB-4 NCs films showed maximum stability. The degradation times for CPB-1, CPB-2, CPB-3, and CPB-4 NCs films were recorded as approximately 60, 120, 180, and 300 min, respectively. All these water stability results show that the addition of OABr and polymer significantly improves the NCs stability *via* effective passivation of NCs surfaces that protect from outside harsh atmosphere.

We also examined the PL stability of these NCs films in different heating and cooling cycles. The high stability is very important for optoelectronic devices as the conduction of charge carriers through the films produces heat. Here, we recorded the percentage of PL intensity of the NCs films that were retained back after heating them to a certain temperature and then cooled down to room temperature. In this case, the PL intensities of the different NCs films were measured at different temperatures during the heating and cooling process. The subsequent changes in PL intensities are shown in Fig. 5d. We observed that while increasing the temperature to 60 °C, the PL intensities of CPB-1, CPB-2, CPB-3, and CPB-4 NCs films were decreased by 70, 55, 53, and 47%, respectively as compared to their emission intensities measured at room temperature. The decrease in PL intensities of these films attributes to the strengthened lattice vibration at higher temperatures, which leads to more non-radiative recombination.[87] Then the films were cooled down to room temperature to complete the first heating–cooling cycle. Interestingly, the PL emission intensities of the films recovered gradually during the cooling process. The retention percentage in PL intensity for CPB-1 NCs films is lowest (*i.e.*, 46%), while it is highest for CPB-4 NCs films (*i.e.*, 95%). The CPB-2 & CPB-3 NCs films show the PL retention percentage as 55 & 89%, respectively for first cycle. The films have not recovered their PL intensities completely due to the degradation of perovskite structure or formation of trap states at higher temperatures.[88] In the second heating–cooling cycle, the PL retention intensities for CPB-1, CPB-2, CPB-3, and CPB-4 NCs films were measured as 21, 35, 41, and 45%, respectively. The retention percentage of PL intensities of all NCs decrease with further heating–cooling cycles. These results indicate that polymer coating also help to improve the heat stability of the NCs.

Further, we measured the contact angle of all NCs films in order to examine the hydrophobicity or the degree of moisture diffusion of the films. The photographic images of contact angles for different films are shown in Fig. 6a–d. The contact angle for CPB-1 NCs film was calculated as 59°, indicating the hydrophilic nature of the film. The contact angles for CPB-2, CPB-3, and CPB-4 NCs films were measured as 68°, 73°, and 82°, respectively. The higher contact angle value for polymer-coated NCs films indicates the increase in hydrophobicity and defensive function to suppress the moisture invasion inside the films due to the presence of polymers coating around the NCs surface.[89,90] Later we compared the film coverage and the local emission properties of silica-coated $CsPbBr_3$ NCs and CPB-4 NCs films by fluorescence microscopy mapping, and corresponding images are shown in Fig. 6e and f, respectively. The fluorescent map of silica-coated NCs evidence highly agglomerated NCs or clustering of the NCs that were detected from the presence of brighter regions with a characteristic size of a few µm. Some places of the film are dark in color which indicates the lack of NCs in those regions. However, the CPB-4 NCs film shows well-distributed particles over the substrate and can't observe any big clusters. This confirms that the polymer coating around the NCs reduces the agglomeration among other NCs and facilitates the growth of smaller, well-dispersed NCs that are necessary for the intake of NCs in cells for bioimaging applications.

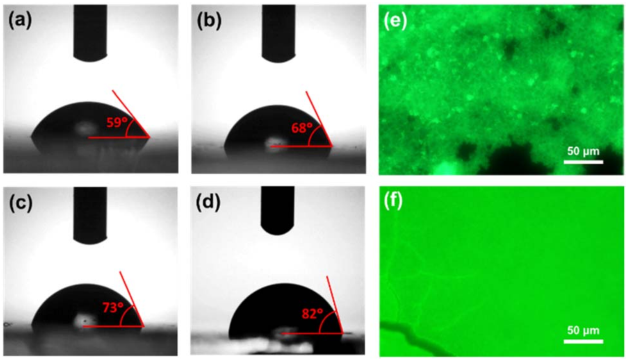

Fig. 6 Contact angle measurement images of (a) CPB-1, (b) CPB-2, (c) CPB-3, and (d) CPB-4 NCs films, respectively. Fluorescence microscopy images of (e) silica-coated $CsPbBr_3$ and (f) CPB-4 NCs films.

We investigated the potential use of silica-coated $CsPbBr_3$ NCs and polymer-coated CPB-4 NCs for bioimaging applications using live-cell confocal microscopy. For this purpose, CHO-K1 mammalian cells were first incubated with silica-coated $CsPbBr_3$ NCs with a dilution ratio of 1 : 100. In order to check the interactions of NCs with sub-cellular organelles, the cells were co-stained with Nonyl-Acridine Orange (mitochondria) and Lysotracker Red (lysosomes). Low uptake of NCs was observed in the cells along with scarce distribution and agglomeration of NCs at certain regions in the cytoplasm (see Fig. 7). In second case, CHO-K1 cells were incubated with CPB-4 NCs at a dilution of 1 : 250 for 1 hour. The live cell confocal images are shown in Fig. 8. The uptake of the NCs were seen in the cells and no notable visible morphological changes were

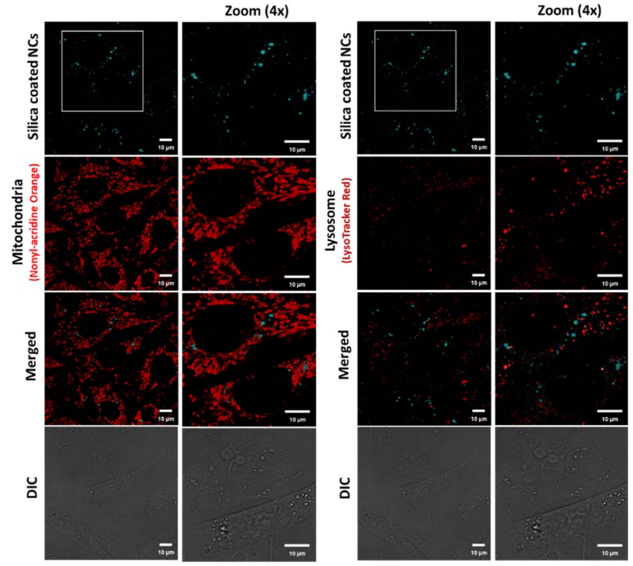

Fig. 7 Bioimaging of silica-coated $CsPbBr_3$ NCs in CHO-K1 cells. The NCs (cyan) are agglomerated in the cytoplasm. Mitochondria stained by Nonyl-Acridine Orange (represented as the pseudo color red) and lysosomes (red) by Lysotracker red.

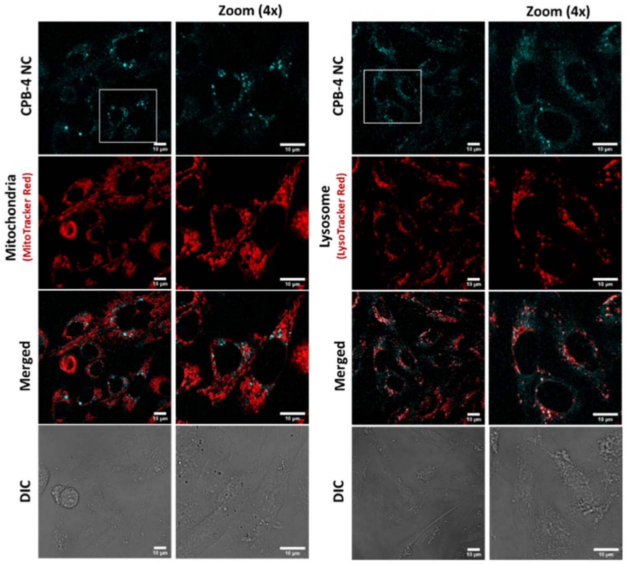

Fig. 8 Bioimaging of CPB-4 NCs in mammalian cells. The NCs (cyan) are internalized by CHO-K1 cells. No evident morphological alterations of mitochondria (red) and lysosomes (red) are observed.

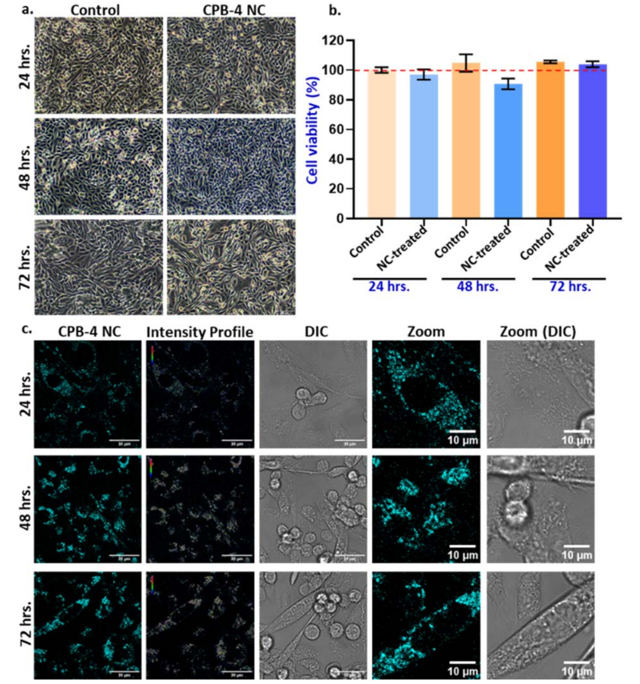

Fig. 9 Effect of long-term incubation of CPB-4 NCs in CHO-K1 cells. (a and b) Cells were treated with CPB-4 NCs at 1 : 250 dilution for 24, 48 and 72 hours. Prolonged exposure of these NCs to cell does not affect the cell viability and proliferation as indicated by MTT assay. (c) The fluorescence property of the NCs was evaluated in long-term incubation periods. The fluorescence of NCs in cells retains upto 72 hours of incubation.

observed in cells suggesting CPB-4 NCs did not cause any cellular toxicity. Further, we went ahead to test whether these NCs are detrimental to sub-cellular organelles or have any possible interactions with them. Towards this, we co-stained the cells for mitochondria (MitoTracker Red) and lysosomes (LysoTracker Red) along with NCs. In both situations, the structural integrity of mitochondria and lysosomes was found to be intact. Also, the intensity of mitochondria and lysosomes was not distorted suggesting that both mitochondria and lysosomes are functional in nature in NCs treated cells.

Finally, we inspected the long-term effect of CPB-4 NCs in cells. Here we incubated the cells for 24, 48, and 72 hours in presence of the NCs and tested the cell viability using MTT assay as shown in Fig. 9. Our results suggest that CPB-4 NCs does not affect the cells viability/proliferation and cell morphology with prolonged incubation up to 3 days (see Fig. 9a and b). Furthermore, the cell viability (as measured by MTT assay) was not affected greatly up to 3 days of NCs incubation. In all the CPB-4 NC-treated cases, the cell viability was greater than 85% as compared to the control (untreated cells). Additionally, we tested the fluorescence properties of the CPB-4 NCs treated cells at the same time points (see Fig. 9c). We observed that the fluorescence of the CPB-4 NCs was retained for up to 3 days of incubation. It seems that the fluorescence intensity of the CPB-4 NCs increases after 24 hours. Therefore, both the cellular uptake and fluorescence efficiency of CPB-4 NCs seem to improve in the cells with longer periods of incubation time (48 and 72 hours). Overall, our data suggest that CPB-4 NCs does not have notable cytotoxicity, and the fluorescence property of the NCs increases with more time of incubation in cells.

Compared to silica-coated $CsPbBr_3$ NCs, CPB-4 NCs are more uniformly distributed in cytoplasm and thereby increase the resolution of imagery that imparts better sensitivity. The silica-coated $CsPbBr_3$ NCs degrade at much faster rate releasing toxic lead contents resulting in cell death whereas compact polymer coating of CPB-4 NCs reduces its degradation in cells and leaching of lead thereby averting cell death.[91,92] At higher concentrations the NCs have detrimental effect on cells. Overall, CPB-4 NCs performed better in terms of cell uptake due to smaller size, with reduced agglomeration and well distributed throughout cytoplasm. The concentration of Pb-ions inside the NCs was maintained less than 5 $\mu g\ mL^{-1}$ that is below the toxicity threshold value, reducing overall cytotoxicity and cell death.[58] Compact coating of polymers avoided leaching of toxic lead thereby reducing cell death. Therefore, we propose that these CPB-4 NCs can be executed for potential bioimaging applications in live cells.

3. Conclusions

In summary, we have synthesized $CsPbBr_3$ NCs *via* LARP synthetic approach in an open atmosphere (relative humidity level >70%). These NCs were encapsulated with different capping ligands and polymer and their optical and structural properties were tested. The XRD diffraction patterns of all NCs reveal mixed phases of $CsPbBr_3$ and Cs_4PbBr_6 perovskite phases. The OAc-OAm capped NCs are not stable in polar solvents which can be a result of the dynamic nature of ligands. However, silica or polymer coating improves the NCs stability due to effective passivation of NCs surface. Silica-coated $CsPbBr_3$ NCs tend to agglomerate among other NCs and become bigger particles, which is detrimental for bioimaging applications. In this regard, we synthesized highly stable, luminescent, and bio-compatible polymer-coated NCs with PLQY more than 80%. The NCs synthesized in presence of both NIPAM and PVP exhibited excellent heat and water stabilities. The FTIR and NMR analysis reveals that PVP polymer is not only adsorbed on NC surface but also bonds with NC surface atoms and NIPAM. These NCs are easily dispersible in water and had a PL retention intensity of 75% after 1 hour in DI water. The overall stability is around 1 week which is favourable for incubation of NCs in biological cell mediums. The higher stability of polymer-coated NCs allows the successful incorporation of these NCs in mammalian Chinese hamster ovary (CHOK1) cells for bioimaging applications.

The enhanced stability of NCs enables incubation in cells at very low concentrations such that the Pb concentration is less than 5 $\mu g\ mL^{-1}$, below toxicity threshold of the respective element thus reducing overall cytotoxicity and cell death. The uptake efficiency of polymer coated NCs is higher as compared to silica-coated NCs. The polymer-coated NCs have lesser cellular toxicity as compared to silica coated NCs. Additionally, the cellular uptake and fluorescence efficiency of polymer coated NCs improve in the cells for longer incubation times. These observations make polymer-coated perovskite NCs as potential candidates for live-cell bioimaging applications.

Author contributions

S. B. and M. R. K. conceived the research idea and planned the experiments. M. R. K. performed the synthesis, characterization, and related experiments. S. K. and T. K. A. equally contributed in the bioimaging part. The manuscript was written with the contributions of all authors. All authors have given approval to the final version of the manuscript. S. B. led the project.

Conflicts of interest

There are no conflicts to declare.

Acknowledgements

This research was supported by the Department of Science and Technology, India for financial support through the DST-INSPIRE Faculty research award (DST/INSPIRE/04/2017/000530). We also acknowledge the ICT-IOC startup research grant for financial support.

Notes and references

1 P. Alivisatos, The use of nanocrystals in biological detection, *Nat. Biotechnol.*, 2004, **22**, 47–52.
2 L. Cao, X. Wang, M. J. Meziani, F. Lu, H. Wang, P. G. Luo, Y. Lin, B. A. Harruff, L. M. Veca, D. Murray, S.-Y. Xie and Y.-P. Sun, Carbon Dots for Multiphoton Bioimaging, *J. Am. Chem. Soc.*, 2007, **129**, 11318–11319.
3 U. Resch-Genger, M. Grabolle, S. Cavaliere-Jaricot, R. Nitschke and T. Nann, Quantum dots *versus* organic dyes as fluorescent labels, *Nat. Methods*, 2008, **5**, 763–775.
4 J. Yao, M. Yang and Y. Duan, Chemistry, Biology, and Medicine of Fluorescent Nanomaterials and Related Systems: New Insights into Biosensing, Bioimaging, Genomics, Diagnostics, and Therapy, *Chem. Rev.*, 2014, **114**, 6130–6178.
5 F. Peng, Y. Su, Y. Zhong, C. Fan, S.-T. Lee and Y. He, Silicon Nanomaterials Platform for Bioimaging, Biosensing, and Cancer Therapy, *Acc. Chem. Res.*, 2014, **47**, 612–623.
6 O. S. Wolfbeis, An overview of nanoparticles commonly used in fluorescent bioimaging, *Chem. Soc. Rev.*, 2015, **44**, 4743–4768.
7 Y. Cai, Z. Wei, C. Song, C. Tang, W. Han and X. Dong, Optical nano-agents in the second near-infrared window for biomedical applications, *Chem. Soc. Rev.*, 2019, **48**, 22–37.
8 M. D. Peterson, L. C. Cass, R. D. Harris, K. Edme, K. Sung and E. A. Weiss, The Role of Ligands in Determining the Exciton Relaxation Dynamics in Semiconductor Quantum Dots, *Annu. Rev. Phys. Chem.*, 2014, **65**, 317–339.
9 M. A. Boles, D. Ling, T. Hyeon and D. V. Talapin, The surface science of nanocrystals, *Nat. Mater.*, 2016, **15**, 141–153.
10 C. Giansante, Library Design of Ligands at the Surface of Colloidal Nanocrystals, *Acc. Chem. Res.*, 2020, **53**, 1458–1467.
11 E. E. Lees, T.-L. Nguyen, A. H. A. Clayton and P. Mulvaney, The Preparation of Colloidally Stable, Water-Soluble, Biocompatible, Semiconductor Nanocrystals with a Small Hydrodynamic Diameter, *ACS Nano*, 2009, **3**, 1121–1128.
12 N. Ma, G. Tikhomirov and S. O. Kelley, Nucleic Acid-Passivated Semiconductor Nanocrystals: Biomolecular Templating of Form and Function, *Acc. Chem. Res.*, 2010, **43**, 173–180.
13 Y. Zhang and A. Clapp, Overview of Stabilizing Ligands for Biocompatible Quantum Dot Nanocrystals, *Sensors*, 2011, **11**, 11036–11055.
14 R. H. H. Neubert, Potentials of new nanocarriers for dermal and transdermal drug delivery, *Eur. J. Pharm. Biopharm.*, 2011, **77**, 1–2.
15 P. Sahandi Zangabad, M. Karimi, F. Mehdizadeh, H. Malekzad, A. Ghasemi, S. Bahrami, H. Zare, M. Moghoofei, A. Hekmatmanesh and M. R. Hamblin, Nanocaged platforms: modification, drug delivery and nanotoxicity. Opening synthetic cages to release the tiger, *Nanoscale*, 2017, **9**, 1356–1392.
16 J. K. Patra, G. Das, L. F. Fraceto, E. V. R. Campos, M. D. P. Rodriguez-Torres, L. S. Acosta-Torres, L. A. Diaz-Torres, R. Grillo, M. K. Swamy, S. Sharma, S. Habtemariam and H.-S. Shin, Nano based drug delivery systems: recent developments and future prospects, *J. Nanobiotechnol.*, 2018, **16**, 71.
17 J. L. West and N. J. Halas, Engineered Nanomaterials for Biophotonics Applications: Improving Sensing, Imaging, and Therapeutics, *Annu. Rev. Biomed. Eng.*, 2003, **5**, 285–292.

18 B. A. Kairdolf, A. M. Smith, T. H. Stokes, M. D. Wang, A. N. Young and S. Nie, Semiconductor quantum dots for bioimaging and biodiagnostic applications, *Annu. Rev. Anal. Chem.*, 2013, **6**, 143–162.

19 Z. Li, Q. Sun, Y. Zhu, B. Tan, Z. P. Xu and S. X. Dou, Ultra-small fluorescent inorganic nanoparticles for bioimaging, *J. Mater. Chem. B*, 2014, **2**, 2793–2818.

20 J. Yan, W. He, N. Li, M. Yu, Y. Du, B. Lei and P. X. Ma, Simultaneously targeted imaging cytoplasm and nucleus in living cell by biomolecules capped ultra-small GdOF nanocrystals, *Biomaterials*, 2015, **59**, 21–29.

21 M. V. Kovalenko, L. Protesescu and M. I. Bodnarchuk, Properties and potential optoelectronic applications of lead halide perovskite nanocrystals, *Science*, 2017, **358**, 745–750.

22 X. He, Y. Qiu and S. Yang, Fully-Inorganic Trihalide Perovskite Nanocrystals: A New Research Frontier of Optoelectronic Materials, *Adv. Mater.*, 2017, **29**, 1700775.

23 Q. A. Akkerman, G. Rainò, M. V. Kovalenko and L. Manna, Genesis, challenges and opportunities for colloidal lead halide perovskite nanocrystals, *Nat. Mater.*, 2018, **17**, 394–405.

24 Y. Wu, X. Li and H. Zeng, Highly Luminescent and Stable Halide Perovskite Nanocrystals, *ACS Energy Lett.*, 2019, **4**, 673–681.

25 Y. Li, X. Zhang, H. Huang, S. V. Kershaw and A. L. Rogach, Advances in metal halide perovskite nanocrystals: Synthetic strategies, growth mechanisms, and optoelectronic applications, *Mater. Today*, 2020, **32**, 204–221.

26 S.-J. Woo, J. S. Kim and T.-W. Lee, Characterization of stability and challenges to improve lifetime in perovskite LEDs, *Nat. Photonics*, 2021, **15**, 630–634.

27 X.-K. Liu, W. Xu, S. Bai, Y. Jin, J. Wang, R. H. Friend and F. Gao, Metal halide perovskites for light-emitting diodes, *Nat. Mater.*, 2021, **20**, 10–21.

28 M. R. Kar, S. Ray, B. K. Patra and S. Bhaumik, State of the art and prospects of metal halide perovskite core@shell nanocrystals and nanocomposites, *Mater. Today Chem.*, 2021, **20**, 100424.

29 W. Chen, S. Bhaumik, S. A. Veldhuis, G. Xing, Q. Xu, M. Grätzel, S. Mhaisalkar, N. Mathews and T. C. Sum, Giant five-photon absorption from multidimensional core-shell halide perovskite colloidal nanocrystals, *Nat. Commun.*, 2017, **8**, 15198.

30 Y. Wang, X. Li, X. Zhao, L. Xiao, H. Zeng and H. Sun, Nonlinear Absorption and Low-Threshold Multiphoton Pumped Stimulated Emission from All-Inorganic Perovskite Nanocrystals, *Nano Lett.*, 2016, **16**, 448–453.

31 J. Chen, K. Žídek, P. Chábera, D. Liu, P. Cheng, L. Nuuttila, M. J. Al-Marri, H. Lehtivuori, M. E. Messing, K. Han, K. Zheng and T. Pullerits, Size- and Wavelength-Dependent Two-Photon Absorption Cross-Section of CsPbBr3 Perovskite Quantum Dots, *J. Phys. Chem. Lett.*, 2017, **8**, 2316–2321.

32 G. Nedelcu, L. Protesescu, S. Yakunin, M. I. Bodnarchuk, M. J. Grotevent and M. V. Kovalenko, Fast Anion-Exchange in Highly Luminescent Nanocrystals of Cesium Lead Halide Perovskites ($CsPbX_3$, X = Cl, Br, I), *Nano Lett.*, 2015, **15**, 5635–5640.

33 L. Protesescu, S. Yakunin, M. I. Bodnarchuk, F. Krieg, R. Caputo, C. H. Hendon, R. X. Yang, A. Walsh and M. V. Kovalenko, Nanocrystals of Cesium Lead Halide Perovskites ($CsPbX_3$, X = Cl, Br, and I): Novel Optoelectronic Materials Showing Bright Emission with Wide Color Gamut, *Nano Lett.*, 2015, **15**, 3692–3696.

34 Z. Yuan, Y. Shu, Y. Tian, Y. Xin and B. Ma, A facile one-pot synthesis of deep blue luminescent lead bromide perovskite microdisks, *Chem. Commun.*, 2015, **51**, 16385–16388.

35 F. Zhang, H. Zhong, C. Chen, X.-G. Wu, X. Hu, H. Huang, J. Han, B. Zou and Y. Dong, Brightly Luminescent and Color-Tunable Colloidal $CH_3NH_3PbX_3$ (X = Br, I, Cl) Quantum Dots: Potential Alternatives for Display Technology, *ACS Nano*, 2015, **9**, 4533–4542.

36 A. Pan, B. He, X. Fan, Z. Liu, J. J. Urban, A. P. Alivisatos, L. He and Y. Liu, Insight into the Ligand-Mediated Synthesis of Colloidal $CsPbBr_3$ Perovskite Nanocrystals: The Role of Organic Acid, Base, and Cesium Precursors, *ACS Nano*, 2016, **10**, 7943–7954.

37 J. De Roo, M. Ibáñez, P. Geiregat, G. Nedelcu, W. Walravens, J. Maes, J. C. Martins, I. Van Driessche, M. V. Kovalenko and Z. Hens, Highly Dynamic Ligand Binding and Light Absorption Coefficient of Cesium Lead Bromide Perovskite Nanocrystals, *ACS Nano*, 2016, **10**, 2071–2081.

38 Q. Zhong, M. Cao, Y. Xu, P. Li, Y. Zhang, H. Hu, D. Yang, Y. Xu, L. Wang, Y. Li, X. Zhang and Q. Zhang, L-Type Ligand-Assisted Acid-Free Synthesis of $CsPbBr_3$ Nanocrystals with Near-Unity Photoluminescence Quantum Yield and High Stability, *Nano Lett.*, 2019, **19**, 4151–4157.

39 K. K. Chan, D. Giovanni, H. He, T. C. Sum and K.-T. Yong, Water-Stable All-Inorganic Perovskite Nanocrystals with Nonlinear Optical Properties for Targeted Multiphoton Bioimaging, *ACS Appl. Nano Mater.*, 2021, **4**, 9022–9033.

40 P. M. Talianov, O. O. Peltek, M. Masharin, S. Khubezhov, M. A. Baranov, A. Drabavičius, A. S. Timin, L. E. Zelenkov, A. P. Pushkarev, S. V. Makarov and M. V. Zyuzin, Halide Perovskite Nanocrystals with Enhanced Water Stability for Upconversion Imaging in a Living Cell, *J. Phys. Chem. Lett.*, 2021, **12**, 8991–8998.

41 C.-Y. Zhong, L. Xiao, J. Zhou, Z. Chen, Y. Chen, Z.-Q. Liu and J. Z. Zhang, Two-photon photoluminescence and bio-imaging application of monodispersed perovskite-in-silica nanocrystals with high biocompatibility, *Chem. Eng. J.*, 2022, **431**, 134110.

42 M. R. Kar, R. Chakraborty, U. Patel, R. Chakraborty, S. Ray, T. K. Acharya, C. Goswami and S. Bhaumik, Impact of Zn-doping on the composition, stability, luminescence properties of silica coated all-inorganic cesium lead bromide nanocrystals and their biocompatibility, *Mater. Today Chem.*, 2022, **23**, 100753.

43 Y.-T. Zeng, Z.-R. Li, S.-P. Chang, A. Ansay, Z.-H. Wang and C.-Y. Huang, Bright $CsPbBr_3$ Perovskite Nanocrystals with

Improved Stability by *In Situ* Zn-Doping, *Nanomaterials*, 2022, **12**, 759.

44 W. Yao, D. Li, H. Wang and L. Yang, Room-temperature synthesis of Mn^{2+}-doped cesium lead halide perovskite nanocrystals *via* a transformation doping method, *J. Mater. Sci.: Mater. Electron.*, 2019, **30**, 180–188.

45 S. Bhaumik, Oriented Attachment of Perovskite Cesium Lead Bromide Nanocrystals, *ChemistrySelect*, 2019, **4**, 4538–4543.

46 D. Baranov, A. Fieramosca, R. X. Yang, L. Polimeno, G. Lerario, S. Toso, C. Giansante, M. D. Giorgi, L. Z. Tan, D. Sanvitto and L. Manna, Aging of Self-Assembled Lead Halide Perovskite Nanocrystal Superlattices: Effects on Photoluminescence and Energy Transfer, *ACS Nano*, 2021, **15**, 650–664.

47 J. Liu, X. Zheng, O. F. Mohammed and O. M. Bakr, Self-Assembly and Regrowth of Metal Halide Perovskite Nanocrystals for Optoelectronic Applications, *Acc. Chem. Res.*, 2022, **55**, 262–274.

48 Z. Lv, Y. Wang, J. Chen, J. Wang, Y. Zhou and S.-T. Han, Semiconductor Quantum Dots for Memories and Neuromorphic Computing Systems, *Chem. Rev.*, 2020, **120**, 3941–4006.

49 G. Ruan, A. Agrawal, A. I. Marcus and S. Nie, Imaging and Tracking of Tat Peptide-Conjugated Quantum Dots in Living Cells: New Insights into Nanoparticle Uptake, Intracellular Transport, and Vesicle Shedding, *J. Am. Chem. Soc.*, 2007, **129**, 14759–14766.

50 P. Zrazhevskiy, M. Sena and X. Gao, Designing multifunctional quantum dots for bioimaging, detection, and drug delivery, *Chem. Soc. Rev.*, 2010, **39**, 4326–4354.

51 A. Reisch and A. S. Klymchenko, Fluorescent Polymer Nanoparticles Based on Dyes: Seeking Brighter Tools for Bioimaging, *Small*, 2016, **12**, 1968–1992.

52 X. T. Zheng, A. Ananthanarayanan, K. Q. Luo and P. Chen, Glowing Graphene Quantum Dots and Carbon Dots: Properties, Syntheses, and Biological Applications, *Small*, 2015, **11**, 1620–1636.

53 S. Bera and N. Pradhan, Perovskite Nanocrystal Heterostructures: Synthesis, Optical Properties, and Applications, *ACS Energy Lett.*, 2020, **5**, 2858–2872.

54 C. Zhang, J. Chen, L. Kong, L. Wang, S. Wang, W. Chen, R. Mao, L. Turyanska, G. Jia and X. Yang, Core/Shell Metal Halide Perovskite Nanocrystals for Optoelectronic Applications, *Adv. Funct. Mater.*, 2021, **31**, 2100438.

55 G. H. Ahmed, J. Yin, O. M. Bakr and O. F. Mohammed, Successes and Challenges of Core/Shell Lead Halide Perovskite Nanocrystals, *ACS Energy Lett.*, 2021, **6**, 1340–1357.

56 Y. Wang, L. Varadi, A. Trinchi, J. Shen, Y. Zhu, G. Wei and C. Li, Spray-Assisted Coil–Globule Transition for Scalable Preparation of Water-Resistant $CsPbBr_3$@PMMA Perovskite Nanospheres with Application in Live Cell Imaging, *Small*, 2018, **14**, 1803156.

57 Z. Lu, Y. Li, W. Qiu, A. L. Rogach and S. Nagl, Composite Films of $CsPbBr_3$ Perovskite Nanocrystals in a Hydrophobic Fluoropolymer for Temperature Imaging in Digital Microfluidics, *ACS Appl. Mater. Interfaces*, 2020, **12**, 19805–19812.

58 S. K. Avugadda, A. Castelli, B. Dhanabalan, T. Fernandez, N. Silvestri, C. Collantes, D. Baranov, M. Imran, L. Manna, T. Pellegrino and M. P. Arciniegas, Highly Emitting Perovskite Nanocrystals with 2-Year Stability in Water through an Automated Polymer Encapsulation for Bioimaging, *ACS Nano*, 2022, **16**(9), 13657–13666.

59 H. Zhang, X. Wang, Q. Liao, Z. Xu, H. Li, L. Zheng and H. Fu, Embedding Perovskite Nanocrystals into a Polymer Matrix for Tunable Luminescence Probes in Cell Imaging, *Adv. Funct. Mater.*, 2017, **27**, 1604382.

60 R. Si, Y.-W. Zhang, L.-P. You and C.-H. Yan, Self-Organized Monolayer of Nanosized Ceria Colloids Stabilized by Poly(vinylpyrrolidone), *J. Phys. Chem. B*, 2006, **110**, 5994–6000.

61 S. Mahalunkar, A. S. Yadav, M. Gorain, V. Pawar, R. Braathen, S. Weiss, B. Bogen, S. W. Gosavi and G. C. Kundu, Functional design of pH-responsive folate-targeted polymer-coated gold nanoparticles for drug delivery and *in vivo* therapy in breast cancer, *Int. J. Nanomed.*, 2019, **14**, 8285–8302.

62 W. Wu, T. Zhou, A. Berliner, P. Banerjee and S. Zhou, Smart Core−Shell Hybrid Nanogels with Ag Nanoparticle Core for Cancer Cell Imaging and Gel Shell for pH-Regulated Drug Delivery, *Chem. Mater.*, 2010, **22**, 1966–1976.

63 X. Zhang, P. Yang, Y. Dai, P. a. Ma, X. Li, Z. Cheng, Z. Hou, X. Kang, C. Li and J. Lin, Multifunctional Up-Converting Nanocomposites with Smart Polymer Brushes Gated Mesopores for Cell Imaging and Thermo/pH Dual-Responsive Drug Controlled Release, *Adv. Funct. Mater.*, 2013, **23**, 4067–4078.

64 K. Haupt, P. X. Medina Rangel and B. T. S. Bui, Molecularly Imprinted Polymers: Antibody Mimics for Bioimaging and Therapy, *Chem. Rev.*, 2020, **120**, 9554–9582.

65 M. R. Kar, U. Patel and S. Bhaumik, Highly stable and water dispersible polymer-coated $CsPbBr_3$ nanocrystals for Cu-ion detection in water, *Mater. Adv.*, 2022, **3**, 8629–8638.

66 T. Hien Nguyen and R. J. Ansell, *N*-isopropylacrylamide as a functional monomer for noncovalent molecular imprinting, *J. Mol. Recognit.*, 2012, **25**, 1–10.

67 S. Bhaumik, S. A. Veldhuis, Y. F. Ng, M. Li, S. K. Muduli, T. C. Sum, B. Damodaran, S. Mhaisalkar and N. Mathews, Highly stable, luminescent core–shell type methylammonium–octylammonium lead bromide layered perovskite nanoparticles, *Chem. Commun.*, 2016, **52**, 7118–7121.

68 S. Ray, A. Mohapatra and S. Bhaumik, Synthesis of highly stable double-coated Zn-doped cesium lead bromide nanocrystals for indium ion detection in water, *Mater. Adv.*, 2022, **3**, 4684–4692.

69 J. Ye, M. M. Byranvand, C. O. Martínez, R. L. Z. Hoye, M. Saliba and L. Polavarapu, Defect Passivation in Lead-Halide Perovskite Nanocrystals and Thin Films: Toward Efficient LEDs and Solar Cells, *Angew. Chem.*, 2021, **60**, 21636–21660.

70 L. Xu, J. Li, T. Fang, Y. Zhao, S. Yuan, Y. Dong and J. Song, Synthesis of stable and phase-adjustable $CsPbBr_3@Cs_4PbBr_6$ nanocrystals *via* novel anion–cation reactions, *Nanoscale Adv.*, 2019, **1**, 980–988.

71 Y. Wang, D. Yu, Z. Wang, X. Li, X. Chen, V. Nalla, H. Zeng and H. Sun, Solution-Grown $CsPbBr_3/Cs_4PbBr_6$ Perovskite Nanocomposites: Toward Temperature-Insensitive Optical Gain, *Small*, 2017, **13**, 1701587.

72 C. Jia, H. Li, X. Meng and H. Li, $CsPbX_3/Cs_4PbX_6$ core/shell perovskite nanocrystals, *Chem. Commun.*, 2018, **54**, 6300–6303.

73 Z. Liu, Y. Bekenstein, X. Ye, S. C. Nguyen, J. Swabeck, D. Zhang, S.-T. Lee, P. Yang, W. Ma and A. P. Alivisatos, Ligand Mediated Transformation of Cesium Lead Bromide Perovskite Nanocrystals to Lead Depleted Cs_4PbBr_6 Nanocrystals, *J. Am. Chem. Soc.*, 2017, **139**, 5309–5312.

74 D. Xu, Q. Wan, S. Wu, Y. Zhao, X. Xu, L. Li and G. He, Enhancing the performance of LARP-synthesized $CsPbBr_3$ nanocrystal LEDs by employing a dual hole injection layer, *RSC Adv.*, 2020, **10**, 17653–17659.

75 E. Tomaszewska, K. Soliwoda, K. Kadziola, B. Tkacz-Szczesna, G. Celichowski, M. Cichomski, W. Szmaja and J. Grobelny, Detection Limits of DLS and UV-vis Spectroscopy in Characterization of Polydisperse Nanoparticles Colloids, *J. Nanomater.*, 2013, **2013**, 313081.

76 Y. Liu, F. Li, L. Qiu, K. Yang, Q. Li, X. Zheng, H. Hu, T. Guo, C. Wu and T. W. Kim, Fluorescent Microarrays of *in Situ* Crystallized Perovskite Nanocomposites Fabricated for Patterned Applications by Using Inkjet Printing, *ACS Nano*, 2019, **13**, 2042–2049.

77 M.-T. Nistor, A. P. Chiriac, C. Vasile, L. Verestiuc and L. E. Nita, Synthesis of hydrogels based on poly(NIPAM) inserted into collagen sponge, *Colloids Surf., B*, 2011, **87**, 382–390.

78 F. Ganachaud, R. Balic, M. J. Monteiro and R. G. Gilbert, Propagation Rate Coefficient of Poly(*N*-isopropylacrylamide) in Water below Its Lower Critical Solution Temperature, *Macromolecules*, 2000, **33**, 8589–8596.

79 J.-T. Yeh, C.-L. Chen, K. S. Huang, Y. H. Nien, J. L. Chen and P. Z. Huang, Synthesis, characterization, and application of PVP/chitosan blended polymers, *J. Appl. Polym. Sci.*, 2006, **101**, 885–891.

80 A. C. F. Rumondor, P. J. Marsac, L. A. Stanford and L. S. Taylor, Phase Behavior of Poly(vinylpyrrolidone) Containing Amorphous Solid Dispersions in the Presence of Moisture, *Mol. Pharm.*, 2009, **6**, 1492–1505.

81 H. Xia, S. Wu, L. Li and S. Zhang, High binding ability ligand controlled formation of $CsPbX_3$ (X = Cl/Br, Br, I) perovskite nanocrystals with high quantum yields and enhanced stability, *RSC Adv.*, 2018, **8**, 35973–35980.

82 B. Li, Y. Zhang, L. Fu, T. Yu, S. Zhou, L. Zhang and L. Yin, Surface passivation engineering strategy to fully-inorganic cubic $CsPbI_3$ perovskites for high-performance solar cells, *Nat. Commun.*, 2018, **9**, 1076.

83 T. Wang, L. Jin, Y. Zhang, Y. Song, J. Li, Y. Gao and S. Shi, *In situ* gelation behavior of thermoresponsive poly(*N*-vinylpyrrolidone)/poly(*N*-isopropylacrylamide) microgels synthesized by soap-free emulsion polymerization, *Polym. Bull.*, 2018, **75**, 4485–4498.

84 S.-W. Kuo, J.-L. Hong, Y.-C. Huang, J.-K. Chen, S.-K. Fan, F.-H. Ko, C.-W. Chu and F.-C. Chang, Star Poly(*N*-isopropylacrylamide) Tethered to Polyhedral Oligomeric Silsesquioxane (POSS) Nanoparticles by a Combination of ATRP and Click Chemistry, *J. Nanomater.*, 2012, **2012**, 749732.

85 S. Cheng and H. Zhong, What Happens When Halide Perovskites Meet with Water?, *J. Phys. Chem. Lett.*, 2022, **13**, 2281–2290.

86 J. Yang, Z. Yuan, X. Liu, S. Braun, Y. Li, J. Tang, F. Gao, C. Duan, M. Fahlman and Q. Bao, Oxygen- and Water-Induced Energetics Degradation in Organometal Halide Perovskites, *ACS Appl. Mater. Interfaces*, 2018, **10**, 16225–16230.

87 F. Zhang, Z. Shi, S. Li, Z. Ma, Y. Li, L. Wang, D. Wu, Y. Tian, G. Du, X. Li and C. Shan, Synergetic Effect of the Surfactant and Silica Coating on the Enhanced Emission and Stability of Perovskite Quantum Dots for Anticounterfeiting, *ACS Appl. Mater. Interfaces*, 2019, **11**, 28013–28022.

88 I. S. Zhidkov, D. W. Boukhvalov, A. F. Akbulatov, L. A. Frolova, L. D. Finkelstein, A. I. Kukharenko, S. O. Cholakh, C.-C. Chueh, P. A. Troshin and E. Z. Kurmaev, XPS spectra as a tool for studying photochemical and thermal degradation in $APbX_3$ hybrid halide perovskites, *Nano Energy*, 2021, **79**, 105421.

89 S. N. Raja, Y. Bekenstein, M. A. Koc, S. Fischer, D. Zhang, L. Lin, R. O. Ritchie, P. Yang and A. P. Alivisatos, Encapsulation of Perovskite Nanocrystals into Macroscale Polymer Matrices: Enhanced Stability and Polarization, *ACS Appl. Mater. Interfaces*, 2016, **8**, 35523–35533.

90 H. Zhu, Y. Ren, L. Pan, O. Ouellette, F. T. Eickemeyer, Y. Wu, X. Li, S. Wang, H. Liu, X. Dong, S. M. Zakeeruddin, Y. Liu, A. Hagfeldt and M. Grätzel, Synergistic Effect of Fluorinated Passivator and Hole Transport Dopant Enables Stable Perovskite Solar Cells with an Efficiency Near 24%, *J. Am. Chem. Soc.*, 2021, **143**, 3231–3237.

91 Y. Jin, S. Kannan, M. Wu and J. X. Zhao, Toxicity of Luminescent Silica Nanoparticles to Living Cells, *Chem. Res. Toxicol.*, 2007, **20**, 1126–1133.

92 P. V. AshaRani, G. Low Kah Mun, M. P. Hande and S. Valiyaveettil, Cytotoxicity and Genotoxicity of Silver Nanoparticles in Human Cells, *ACS Nano*, 2009, **3**, 279–290.